Geosciences
Geociências

# Petrography and geochemistry of the Pedra Dourada Granulite, southeastern Minas Gerais, Brazil

http://dx.doi.org/10.1590/0370-44672014690192

**Kassia de Souza Medeiros Marinho**
Professora Substituta
Universidade Federal de Ouro Preto – UFOP
Escola de Minas
Departamento de Geologia
Ouro Preto – Minas Gerais – Brasil
kassiamedeiros@yahoo.com.br

**Hanna Jordt-Evangelista**
Professora Titular
Universidade Federal de Ouro Preto – UFOP
Escola de Minas
Departamento de Geologia
Ouro Preto – Minas Gerais – Brasil
hanna@degeo.ufop.br

**Marcelo de Souza Marinho**
Pesquisador em Geociências
Serviço Geológico do Brasil – CPRM
Superintendência Regional de Belo Horizonte
Belo Horizonte - Minas Gerais - Brasil
marcelo.marinho@cprm.gov.br

## Abstract

The Pedra Dourada Granulite (PDG) occurs at the southeastern portion of the Araçuaí Belt, north of the town of Ponte Nova. It comprises bodies up to 45 km$^2$ inserted into amphibolite-facies gneisses of the Mantiqueira Complex. Motivated by the discrepancy of metamorphic grade with surrounding rocks, this paper presents results of the petrographic and geochemical investigation of the PDG. The unit is comprised of meta-igneous and metasedimentary rocks. Meta-igneous rocks dominate and include felsic granulites (biotite ± garnet-bearing and orthopyroxene-bearing) and subordinate mafic granulites. Metasedimentary rocks are aluminous granulites with Al-rich mineral assemblages (garnet, sillimanite, spinel). Geochemical data show that most of felsic protoliths are peraluminous rocks including granites, granodiorites and diorites of calc-alkaline character, chemically similar to granitoids of convergent tectonic settings. Mafic protoliths are metaluminous rocks comprised of gabbros and subordinate diorites of tholeiitic affinity, compositionally similar to plate margin basalts. Aluminous protoliths may be peraluminous pelitic rocks and wackes, analogous to sediments from convergent environments. The mineral assemblages indicate that these rocks were metamorphosed under medium-*P* granulite-facies conditions. Coronitic garnet textures suggest a near-isobaric cooling (IBC-path) after metamorphic peak.

**Keywords:** granulites, geochemistry, Pedra Dourada Granulite, Mantiqueira Complex, Araçuaí Belt.

## 1. Introduction

The Pedra Dourada Granulite (PDG) is located in the southeastern portion of the Araçuaí Belt, which was defined by Almeida (1977) as a Brasiliano fold-thrust belt developed along the southeastern edge of the São Francisco Craton. This belt is now viewed as the external domain of the Araçuaí Orogen (Alkmim *et al.*, 2007).

The Araçuaí Orogen encompasses the entire region between the São Francisco Craton and the Brazilian continental margin and is roughly limited by the 15° and 21° S parallels. This orogen displays an arbitrary boundary with the Ribeira Orogen to the south (Pedrosa-Soares & Wiedemann-Leonardos, 2000) (Figure 1a). The Araçuaí Orogen is subdivided by the Abre Campo Shear Zone into two tectonic domains – the internal (eastern) and the external (western) (Figure 1b). The internal domain corresponds to the crystalline core of the orogen and comprises high amphibolite to granulite facies rocks of the Juiz de Fora Complex (Alkmim *et al.,* 2007).

The external domain, which is correlated to the Araçuaí Belt, is dominantly composed of greenschist- to amphibolite-facies rocks. In southeastern State of Minas Gerais, this belt encompasses a Paleoproterozoic basement, represented by the Mantiqueira Complex, and supracrustal units (*e.g.* Grupo Dom Silvério) (Peres *et al.*, 2004) (Figure 1b). The Mantiqueira Complex is mostly comprised of amphibolite-facies orthogneisses (Noce *et al.,* 2007). The main exceptions consist of two granulite terrains that occur between the southeastern edge of São Francisco Craton and Abre Campo Shear Zone. The western terrain corresponds to the Acaiaca Complex (AC) (Jordt-Evangelista, 1984,1985; Jordt-Evangelista & Muller, 1986a, 1986b; Teixeira *et al.*, 1987; Medeiros Júnior, 2009; Medeiros Júnior & Jordt-Evangelista, 2010). The other is the PDG, originally called Córrego Pedra Dourada Granulite by Brandalise (1991). This unit is located east of the metavolcanosedimentary sequence of the Dom Silvério Group, in the region of the Dom Silvério, Rio Doce and Sem Peixe towns (Peres, 2000) (Figure 1b).

Unlike the AC, the PDG has been little investigated from the petrogenetic point of view. This paper presents and discusses field, petrographic and geochemical data of the PDG. This study aims to contribute to the knowledge of the constitution and evolution of the basement of the Araçuaí Orogen.

## 2. Materials and methods

The spatial distribution of the PDG was defined based on 120 geological stations, in which 72 stations were visited during the field studies from this work. The other field data comes from studies of Jordt-Evangelista (1992, 1996), Alcântara & Machado (2010) and Melo & Maia (2010). The petrographic and microstructural characterization was based on the description of 102 thin sections under polarized light microscope. Whole-rock geochemical analyses were carried out on 20 representative samples of the granulites. These samples were crushed and milled at the Departamento de Geologia of the Universidade Federal de Ouro Preto. Major and trace element concentrations were determined using Inductively Coupled Plasma Emission Spectroscopy (ICP-ES) at the ACME Analytical Laboratory LTDA, Canada. The samples from this study were combined with 17 published rock compositions by Jordt-Evangelista (1996).

## 3. Field characteristics and lithological constitution

The PDG occurs as a large body in the central part of the study area and also as isolated outcrops located in the northern and southern portions of the study area (Figure 2). The field studies show that the occurrence area of the PDG is larger than originally defined by Brandalise (1991).

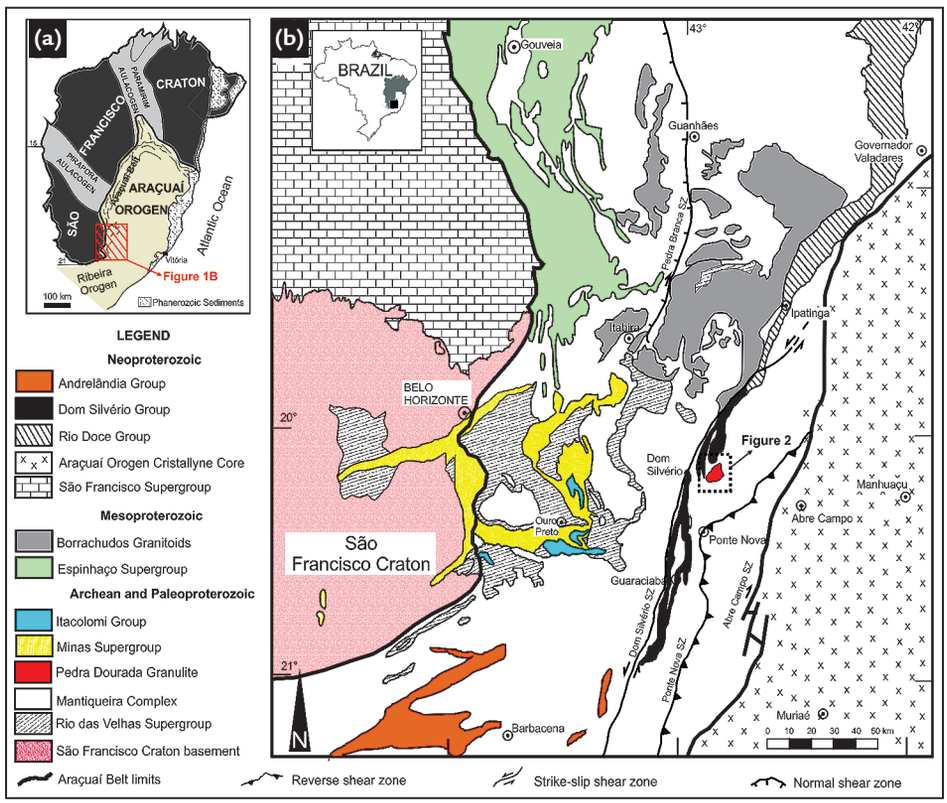


Figure 1
Geotectonic setting of the PDG.
a) The Araçuaí Orogen and adjacents units (São Francisco Craton and Ribeira Orogen). The hatched rectangle corresponds to Figure 1b. Modified from Pedrosa-Soares *et al.* (2007);
b) Regional geologic map of the Araçuaí Belt showing the location of the PDG.The dotted rectangle corresponds to Figure 2. Modified from Peres *et al.* (2004).

The PDG comprises meta-igneous and metasedimentary rocks of granulite-facies. The meta-igneous granulites dominate and include felsic granulites from granite-tonalitic to charnokite-enderbitic composition and less abundant mafic granulites of gabbroic composition. The metasedimentary rocks are aluminous granulites.

The contacts between felsic and mafic granulites are variable. The occurrence of the mafic granulites as rounded, sub-angular or lens-shaped xenoliths in the felsic granulites is common (Figure 3a). However, dominantly mafic outcrops intruded by felsic rocks are also found. The two lithologies also coexist as alternating felsic and mafic bands of few centimeters thick. These bands occur as folded or showing diffuse contacts (Figure 3b). No contacts between aluminous granulites and orthogranulites were observed.

The felsic and the mafic granulites may show both as well as isotropic textures as millimetric to centimetric mineralogical banding, whilst the aluminous granulite exhibits a prominent banding (Figure 3c). Overall, the granulites show a mylonitic foliation parallel to the compositional banding. Furthermore, centimetric scale S-C shear zones were observed in some outcrops.

The granulite-facies rocks also present partial melting features defined by the presence of quartz-feldspathic leucossomes. The textures vary from schlieren, schollen (Figure 3d), fleck (Figure 3e) to phlebitic (Figure 3f). The last occurs predominantly in aluminous granulites while the others are typically found on metaigneous rocks. The leucossome may also contain mafic anhydrous or hydrous mineral phases, like hornblende in mafic granulites (Figure 3e) or garnet in aluminous varieties.

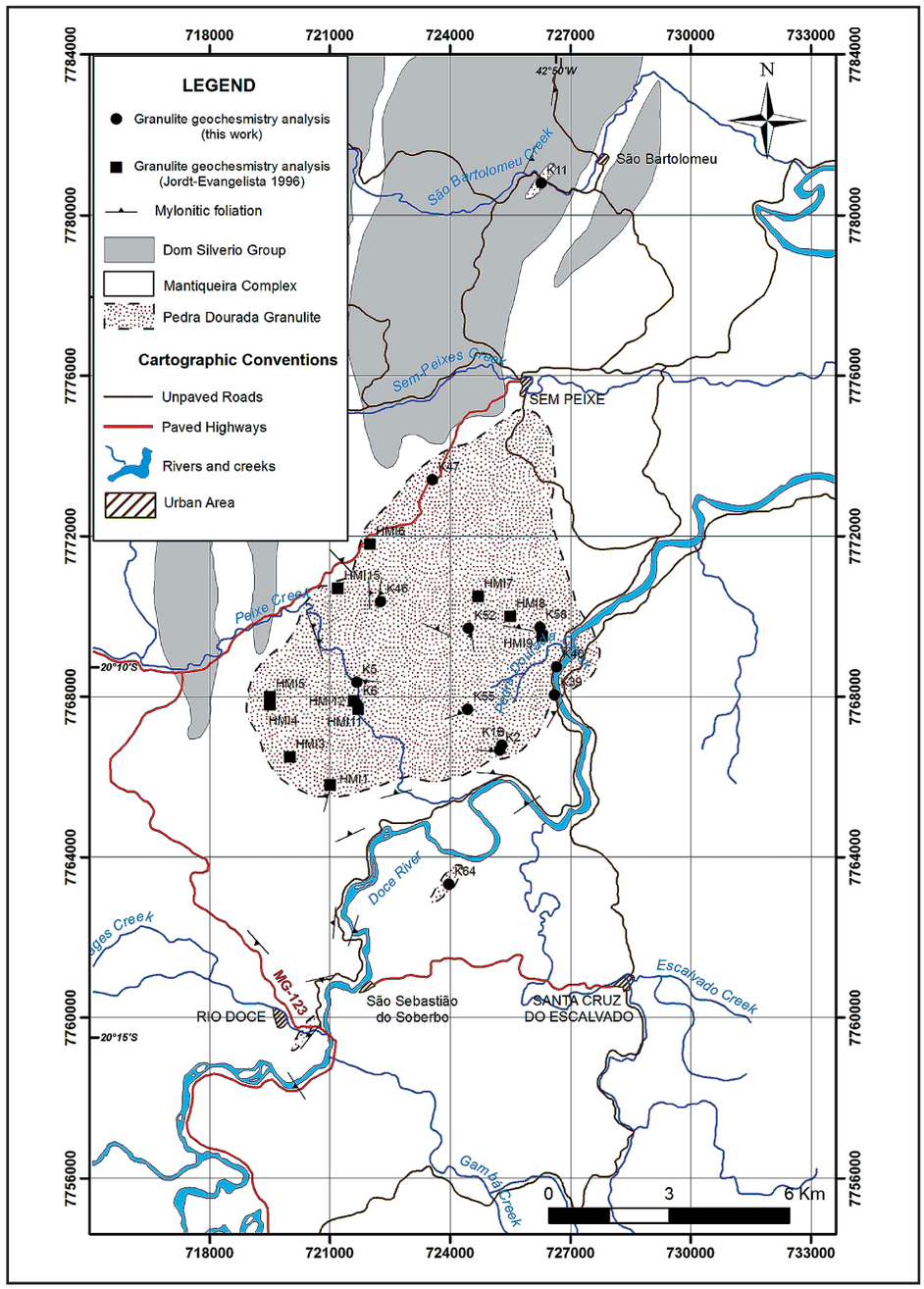


Figure 2
Map of the study area with location of the PDG and the analyzed granulite samples. Modified from Peres (2000)

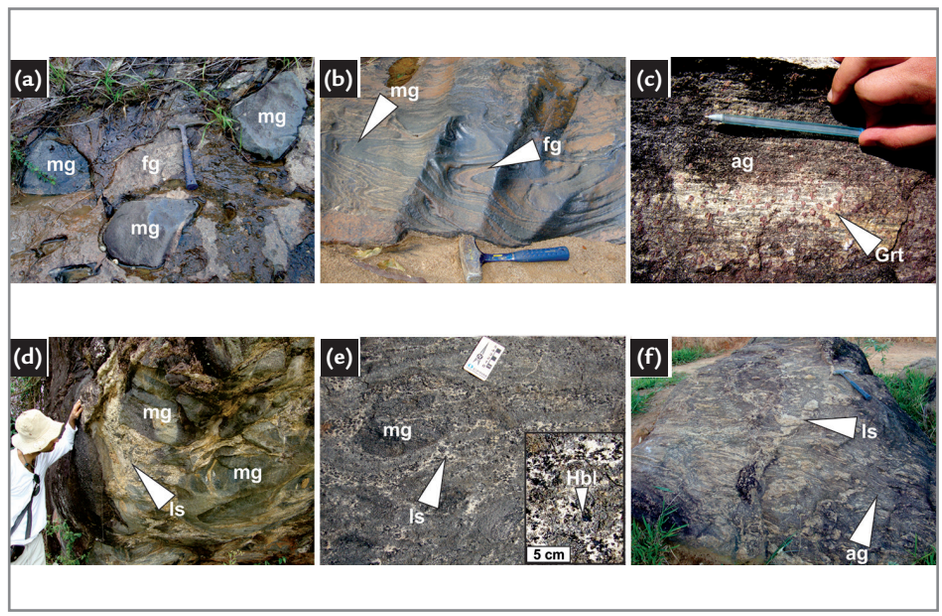


Figure 3
Field aspects of the PDG (geological station in brackets). a) Mafic granulite xenoliths in felsic granulite (K6). b) Folded banding defined by felsic and mafic granulites (K6). c) Aluminous granulite showing millimetric banding and garnet porphyroblasts (K46). d) Schollen structure marked by mafic granulite blocks embedded in leucossome (K11). e) Fleck structure associated to mafic granulite consisting of hornblende cores surrounded by leucossome (K52); (f) Aluminous granulite showing a phlebitic structure characterized by irregular veins of leucossome (K58). Abbreviations: mg-mafic granulite; fg-felsic granulite; ag-aluminous granulite; Grt-garnet; ls-leucossome; Hbl-hornblende.

## 4. Petrography

### Felsic granulites

Felsic granulites are the most abundant granulite-facies rocks in the study area. According to the mafic mineral content, these granulites were subdivided into two groups:

(i) biotite ± garnet-bearing felsic granulites, compositionally belonging to granite-tonalite series, and

(ii) orthopyroxene-bearing felsic granulites, belonging to charnockite-enderbite series.

Biotite ± garnet-bearing felsic granulites display a prevalent inequigranular granoblastic fabric. This lithotype comprises coarse-grained porphyroclasts embedded in a fine- to medium-grained matrix. It is characterized by the mineral assemblage orthoclase + plagioclase + quartz + biotite ± garnet. Zircon, titanite, apatite, allanite, monazite and opaque minerals are the common accessory minerals, plus secondary minerals like chlorite, scapolite, sericite, epidote and carbonate.

Orthoclase (15 - 55% vol) and plagioclase (10 - 45%) occur both as porphyroclasts and as matrix constituent. Porphyroclasts consist of anhedral to subhedral grains with interlobate or ameboid boundaries, suggesting grain boundary migration recrystallisation. They commonly exhibit perthitic (alkali-feldspar) and antiperthitic (plagioclase) exsolutions (Figure 4a) and also show evidences for intracrystalline deformation, like undulose extinction and deformation twins (plagioclase). Matrix grains exhibit anhedral crystal shape and often define core-and-mantle structures in porphyroclasts. Quartz (20 - 35%) occurs as anhedral grains and may be equant or elongate. The grains form the matrix or compose monomineralic ribbons that wrap around feldspar porphyroclasts. The main deformation microstructures are undulose extinction, deformation bands and subgrains, which sometimes define chessboard-type extinction. Biotite (1 - 15%) is reddish-brown ($X_{Mg}$ = 0.57 and 0.33 apfu of Ti) and displays a weak orientation. Smaller secondary flakes are light-green and occur filling fractures in garnet or surrounding this mineral. Garnet (0-5%) may occur as two generations. The primary is characterized by rounded porphyroblasts of $alm_{69,1}prp_{23,0}grs_{4,6}sps_{3,3}$ and contains quartz and feldspars inclusions. The late garnet forms symplectitic intergrowth with opaque minerals.

Orthopyroxene-bearing felsic granulites display inequigranular granoblastic fabric (Figure 4b). This lithotype comprises coarse-grained feldspar porphyroclasts surrounded by a fine to medium-grained matrix. It's characterized by the mineral assemblage plagioclase + orthoclase + quartz + orthopyroxene + biotite ± clinopyroxene ± garnet ± hornblende. Zircon, titanite, apatite, monazite and opaque minerals are the main accessory minerals, plus secondary minerals like chlorite, cummingtonite, epidote and sericite.

Plagioclase (25 - 50% vol), orthoclase (<1 - 45%) and quartz (15 - 35%) are microstructurally similar to those described above. Plagioclase is andesine ($An_{42-43}$) and orthoclase has a composition of $An_1Ab_{10}Or_{89}$. Orthopyroxene (1 - 18%) is Fe-hypersthene ($En_{46-48}$) and shows an anhedral to subhedral crystal shape and evidences of intracrystalline deformation, *e.g.* undulose extinction. However, most grains are partially or totally replaced by fine-grained aggregates of biotite ± cummingtonite ± quartz ± opaque minerals. Biotite (<1 – 20%) is reddish-brown ($X_{Mg}$ = 0.52 and 0.55-0.58 apfu of Ti) and displays undulose extinction. A secondary generation is greenish-brown and replaces orthopyroxene. Clinopyroxene (0 - 12%) is usually better preserved than orthopyroxene but also exhibits replacement by symplectitic intergrowths of quartz + amphiboles. Garnet (0-10%) is $alm_{65,4}grs_{18,5}prp_{12,0}sps_{4,0}uv_{0,1}$ and may compose symplectitic intergrowth with ilmenite or forms coronas around plagioclase (Figure 4c). Hornblende (0 - 8%) occurs both as individual brownish-green crystals of ferropargasite (15eNK estimate, Leake *et al.*, 1997) as in aggregates replacing pyroxenes.

### Mafic granulites

Mafic granulites are the second most abundant granulite-facies rock in the study area. They have a gabbroic composition and display inequigranular granoblastic fabric. This lithotype is composed by the mineral assemblage plagioclase + biotite ± orthopyroxene ± clinopyroxene ± hornblende ± quartz ± garnet (Figure 4d). Zircon, titanite, apatite, allanite and opaque minerals are the common accessory minerals, plus secondary minerals like actinolite, cummingtonite, epidote, scapolite and sericite.

Plagioclase (15 - 40% vol) is andesine ($An_{41-43}$) and occurs as anhedral to subhedral antiperthitic grains. The main deformation microstructures are undulose extinction, deformation twins, subgrains and core-and-mantle structures. Orthopyroxene (0 - 35%) is hypersthene ($En_{56-57}$) and shows anhedral to subhedral crystal shape and is partially or totally replaced by fibrous aggregates of biotite and/or cummingtonite (Figure 4e). Clinopyroxene (0 - 30%) is diopside ($Wo_{47}En_{39}Fe_{14}$) and occurs both in granular aggregates with orthopyroxene or as coronas around this mineral. Commonly clinopyroxene exhibits replacement by actinolite and/or hornblende. Both biotite (<1 – 30%) and hornblende (0 – 45%) occur in two generations. The primary consists of large reddish-brown crystals of biotite ($X_{Mg}$ = 0.60-0.62 and 0.44-0.45 apfu of Ti) and brownish-green crystals of edenite (15eNK estimate, Leake *et al.*, 1997). The secondary generation occurs as fine-grained aggregates replacing pyroxenes. Quartz (<1 - 15%) usually forms monomineralic aggregates and displays deformation microstructures like undulose extinction and chessboard subgrains. Garnet (0 - 8%) has a composition $alm_{58,5}prp_{19,5}grs_{18,5}sps_{3,4}uv_{0,1}$ and may constitute symplectitic intergrowth with ilmenite or coronitic textures at pyroxene-plagioclase contacts (Figure 4f).

### Aluminous granulites

Aluminous granulites are characterized by the abundance of Al-rich minerals like garnet and biotite and by the presence of sillimanite and spinel, which occur only enclosed in garnet. The rock displays an inequigranular granoblastic to lepidoblastic fabric, characterized by coarse-grained garnet and orthopyroxene porphyroblasts, which are embedded in a fine- to medium-grained matrix. This granulite is composed by the main mineral assemblage garnet +

plagioclase + quartz + biotite ± orthoclase ± orthopyroxene. Zircon, spinel, sillimanite, apatite and opaque minerals are the common accessory minerals, plus secondary minerals like chlorite, epidote and sericite.

Garnet (9 – 40% vol) occurs in two generations. The primary generation ($alm_{63}prp_{30}grs_5sps_2$) consists of poikiloblastic anhedral porphyroblasts of up to 2 cm and contains fine-grained rounded or amoeboid inclusions of all other main minerals, besides acicular sillimanite and anhedral spinel (Figure 4g). The secondary generation ($alm_{67}prp_{21}grs_8sps_3uv_1$) forms symplectitic coronas around the primary garnet and also around ilmenite (Figure 4h). Plagioclase (15 – 25%) is oligoclase-labradorite ($An_{24-51}$) and occurs mainly as antiperthitic porphyroclasts, which exhibit interlobate or ameboid grain boundaries and evidences for intracrystalline deformation, like undulose extinction and deformation twins. Orthoclase (0 – 40%) has a composition $An_1Ab_8Or_{91}$ and often occurs as perthitic porphyroclasts. Quartz (10 – 30%) constitutes the matrix or occurs in monomineralic ribbons and shows the same deformation microstructures already described for others granulites. Biotite (2 – 25%) is reddish-brown ($X_{Mg}$ = 0.60-0.74 and 0.43-0.61 apfu of Ti) and defines the penetrative foliation which wraps around porphyroblasts and porphyroclasts. The grains show deformation features like undulose extinction and kink bands. A secondary generation occurs filling fractures in orthopyroxene or surrounding this mineral. Orthopyroxene (0 – 30%) is hypersthene ($En_{57-66}$). It occurs as anhedral porphyroblasts and shows the same deformation features as biotite (Figure 4i). Green spinel (<1%) has an average chemical formula $(Mg_{0,3}Fe_{0,5}Zn_{0,2})(Al_{1,9}Cr_{0,1})O_4$. Due to the prevalence of Fe content, this spinel was classificated as hercynite (Figure 4g).

## 5. Geochemistry

### Felsic granulites

Felsic granulites are comprised of intermediate to acid rocks (58.32 – 76.14% $SiO_2$) (Table 1). In the TAS diagram (Cox *et al.,* 1979 modified by Wilson, 1989), most of the biotite ± garnet-bearing felsic granulites plot within the granite field, with a few in the granodiorite field, while most of the orthopyroxene-bearing felsic granulites fall in the granodiorite field, with some of them in the diorite and granite field. According the same diagram, the felsic granulites belong to the subalkaline/tholeiitic series (Figure 5a).

In the AFM plot of Irvine & Baragar (1971), the felsic granulites scatter around a calc-alkaline trend (Figure 5b). The most differentiated terms, *i.e.*, those that plot near the vertex A ($Na_2O + K_2O$), correspond to biotite ± garnet-bearing felsic granulites. Regarding the aluminum saturation, the biotite ± garnet-bearing felsic granulites are peraluminous rocks, with Shand's index between 1.02 and 1.24. The orthopyroxene-bearing felsic granulites, in turn, plot between the fields of metaluminous and peraluminous rocks, with Shand's index range from 0.87 to 1.08 (Figure 5c).

According to the geochemical classification of Frost *et al.* (2001) for granitic rocks (not shown in this paper) the felsic granulites are magnesian granitoids and belong to the calcic and calc-alkaline series. The same authors have associated these chemical signatures with Cordilheran-type batholiths, island arcs plutons and plagiogranites.

The tectonic setting of the felsic granulites was characterized based on tectonic discrimination diagrams for granitoids. In the Nb *vs*. Y diagram of Pearce *et al*. (1984), most of the felsic granulites plot within the Volcanic arc + Syn-collisional granitoids field (Figure 5e). The $R_1$–$R_2$ diagram of De La Roche *et al*. (1980) with geotectonic implications after Batchelor & Bowden (1985) suggests that a

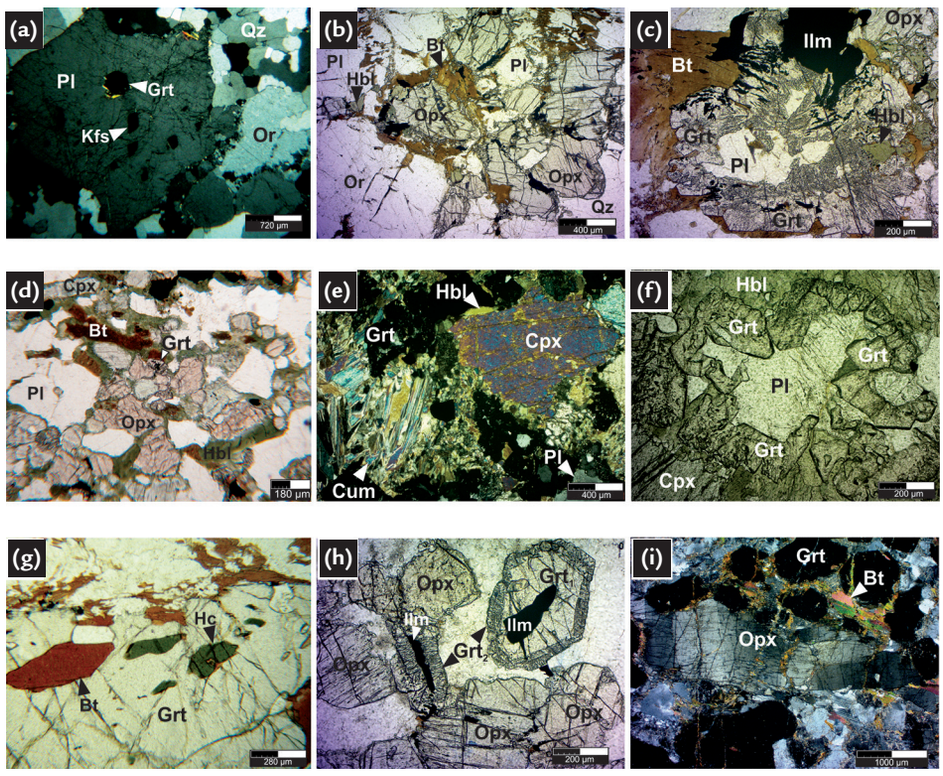


Figure 4
Photomicrographs of the granulite-facies rocks. A-C – Felsic granultes. a) Antiperthitic porphyroclastic plagioclase with garnet inclusion, besides perthitic orthoclase of biotite ± garnet-bearing felsic granulite; b) Mineral assemblage of the orthopyroxene-bearing felsic granulite; c) Coronitic texture defined by symplectitic garnet around plagioclase in orthopyroxene--bearing felsic granulite; D-F – Mafic granulites. d) Granoblastic fabric. e) Cummingtonite pseudomorph after orthopyroxene. f) Corona of garnet around plagioclase; G-I – Aluminous granulites. g) Biotite and hercinite spinel inclusions in porphyroblastic garnet; h) Corona of symplectitic garnet around earlier garnet and ilmenite; i) Kink band in orthopyroxene. Abbreviations: Kfs-alkali-feldspar; Pl-plagioclase; Or-orthoclase; Grt-garnet; Qz-quartz; Ilm-ilmenite; Hbl-hornblende; Bt-biotite; Opx-orthopyroxene; Cpx-clinopyroxene; Cum-cummingtonite; Hc-hercynite.

majority of the felsic granulites have been derived from Pre-collision granitoids, although some samples plot in the Syn-collision and Mantle fractionates fields (Figure 5f). According to the tectonic discrimination scheme of Maniar & Piccoli (1989) (not shown in this paper), the felsic granulites could have been derived from continental arc granitoids (CAG), island arc granitoids (IAG) or continental collison granitoids (CCG).

## Mafic granulites

Mafic granulites comprise basic to intermediate rocks (46.76 – 56.20% $SiO_2$) (Table 1). In the TAS diagram, most of these granulites plot within the gabbro field and few of them in the diorite field. According the same diagram, they belong to the subalkaline/tholeiitic series (Figure 5a).

The AFM diagram shows a tholeiitic signature for most mafic granulites, except for two samples that fall within the calc-alkaline field (Figure 5b). According the Shand's diagram, all these granulites are metaluminous rocks, with ACNK values between 0.48 and 0.85 (Figure 5c).

The tectonic environment of the mafic granulites was characterized based on tectonic discrimination diagrams for basaltic rocks. According the Ti/Y *vs*. Zr/Y diagram of Pearce & Gale (1977), which separates Within-plate basalts and Plate margin basalts, all the mafic granulites show a geochemical signature consistent with Plate margin basalts (Figure 5g). In the ternary diagram of Meschede (1986), the mafic samples disperse in the fields of the E-type MORB – enriched in incompatible trace elements, Within-plate tholeiites + Island arc basalts, and N-type MORB – depleted in incompatible trace elements + Island arc basalts (Figure 5h). Again, no sample presents an exclusive intraplate basalt signature.

## Aluminous granulites

Aluminous granulites comprise basic, intermediate and acid rocks (49.83 – 73.62% $SiO_2$) (Table 1). The Al content ranges from 12.95 to 16.57% and the Shand's diagram shows that all the samples are peraluminous rocks, with ACNK between 1.14 and 2.02 (Figure 5c).

The protoliths were characterized based on the discriminant diagram of Herron (1988), which relates $\log(Fe_2O_3^{(t)}/K_2O)$ *vs*. $\log(SiO_2/Al_2O_3)$ (Figure 5d). According to this diagram, three samples have geochemical characteristics of Fe-shale and one of them has characteristics of wacke.

The tectonic environment of the aluminous granulites was characterized according to the tectonic discrimination diagram for sandstones and argillites of Roser & Korsch (1986), which is based on the $K_2O$, $Na_2O$ and $SiO_2$ content. This scheme suggests an oceanic island arc margin setting for three pelitic rocks and an active continental margin setting for the wacke sample (Figure 5i).

## 6. Discussion

The field work showed that the granulite-facies rocks exhibit evidence for medium- to high-grade deformation, as manifested by folded banding and mylonitic fabric. At the microscope scale, high-grade deformation is characterized by lobates and amoeboid boundaries in quartz-feldspar grains and also chessboard subgrains in quartz. Medium-grade evidence is represented by core-and-mantle structures in feldspars wrapped by quartz ribbons.

The biotite ± garnet-bearing felsic granulites, despite the absence of orthopyroxene, were interpreted as belonging to the granulite-facies due the predominance of orthoclase instead microcline, the antiperthitic plagioclase, the Ti-rich biotite, the absolute absence of primary moscovite and, finally, the associated occurrence in some outcrops with typical mafic granulites. The orthopyroxene-bearing felsic granulites show the same features as the former, besides the orthopyroxene content. The main reaction texture observed in this rock is the symplectitic coronas of garnet and ilmenite around plagioclase. The origin of coronal garnet has been a subject of debate. Sen & Battacharya (1993) opine that a garnet-forming reaction is triggered during retrograde metamorphism as a consequence of near-isobaric cooling (IBC-path). On the other hand, Maji *et al*. (2008) advocate a prograde growth of garnet at the expense of plagioclase + ilmenite ± biotite ± hornblende ± quartz.

On the mafic rocks, the granulite-facies metamorphism is characterized by the paragenesis plagioclase + orthopyroxene + clinopyroxene, which is typical of medium-*P* granulite-facies metabasites (Green & Ringwood, 1967 *in* Yardley, 2004). However, in some mafic granulites only orthopyroxene occurs, while in others only clinopyroxene is found. According to Best (2003), at higher P, orthopyroxene is consumed in garnet-forming reactions as orthopyroxene + plagioclase → garnet + quartz and orthopyroxene + plagioclase → garnet + clinopyroxene + quartz. The former reaction may have generated the coronitic garnet on orthopyroxene-plagioclase contacts, while the latter may have originated the clinopyroxene coronas on orthopyroxene. Harley (1989) associates both reaction textures to retrograde IBC-paths.

On the aluminous granulites, in turn, the high-grade metamorphic event is registered by mineral assemblages with orthoclase, garnet, orthopyroxene, spinel and sillimanite, which characterize moderate-*P* conditions. According to Harley (1989), the symplectitic garnet coronas found around earlier garnet is indicative of an IBC-path in pelitic granulites.

Table 1- Part I - Chemical analyses of selected samples of the Pedra Dourada Granulite.

**Major and minor elements (weight %)**

| Sample | Lithotype | $SiO_2$ | $TiO_2$ | $Al_2O_3$ | $Fe_2O_3$ | MnO | MgO | CaO | $Na_2O$ | $K_2O$ | $P_2O_5$ | $Cr_2O_3$ | LOI | Total |
|---|---|---|---|---|---|---|---|---|---|---|---|---|---|---|
| K5C2 | Bt-grt felsic granulites | 75.74 | 0.14 | 13.90 | 1.02 | 0.01 | 0.34 | 2.87 | 4.28 | 0.77 | 0.03 | 0.002 | 0.70 | 99.90 |
| K52A | | 70.71 | 0.40 | 14.05 | 3.25 | 0.04 | 0.83 | 2.19 | 2.55 | 4.83 | 0.12 | <0.002 | 0.70 | 99.91 |
| K64A | | 70.09 | 0.38 | 14.74 | 3.03 | 0.02 | 1.22 | 2.34 | 3.62 | 2.97 | 0.05 | 0.003 | 1.20 | 99.90 |
| HMI15B* | | 67.72 | 0.58 | 15.51 | 3.85 | 0.05 | 1.21 | 3.37 | 2.93 | 3.86 | 0.18 | - | - | 99.26 |
| HMI7A* | | 72.14 | 0.35 | 14.73 | 2.92 | 0.04 | 0.72 | 1.93 | 3.63 | 2.43 | 0.06 | - | - | 98.95 |
| HMI12G* | | 73.80 | 0.01 | 14.6 | 1.14 | 0.04 | 0.22 | 1.36 | 2.88 | 5.51 | 0.04 | - | - | 99.60 |
| HMI12C* | | 74.49 | 0.03 | 14.47 | 0.71 | 0.02 | 0.21 | 1.18 | 2.71 | 6.08 | 0.04 | - | - | 99.94 |
| HMI6D* | | 75.33 | 0.21 | 13.21 | 1.16 | 0.02 | 0.86 | 2.09 | 3.28 | 2.84 | 0.05 | - | - | 99.05 |
| HMI11C* | | 76.14 | 0.15 | 12.27 | 2.44 | 0.09 | 0.78 | 0.71 | 1.68 | 5.38 | 0.03 | - | - | 99.67 |
| K1B2 | Opx felsic granulites | 66.11 | 0.61 | 15.74 | 4.55 | 0.07 | 1.70 | 4.17 | 3.24 | 2.58 | 0.17 | 0.007 | 0.70 | 99.89 |
| K2E | | 61.92 | 0.86 | 16.64 | 7.01 | 0.10 | 2.26 | 4.64 | 3.44 | 1.97 | 0.25 | 0.004 | 0.60 | 99.87 |
| K11A | | 65.11 | 0.61 | 15.19 | 5.41 | 0.08 | 1.85 | 4.45 | 2.99 | 3.00 | 0.15 | 0.004 | 0.80 | 99.90 |
| K40B | | 70.51 | 0.29 | 14.59 | 3.07 | 0.06 | 1.24 | 2.64 | 3.56 | 3.39 | 0.09 | 0.005 | 0.30 | 99.87 |
| K55A | | 60.19 | 0.57 | 17.82 | 6.54 | 0.12 | 2.81 | 5.30 | 3.91 | 0.91 | 0.32 | 0.007 | 1.20 | 99.88 |
| HMI6C | | 66.00 | 0.72 | 15.95 | 4.95 | 0.08 | 1.42 | 3.62 | 3.57 | 2.58 | 0.21 | <0.002 | 0.50 | 99.96 |
| HMI8A1 | | 70.91 | 0.36 | 14.98 | 2.31 | 0.03 | 0.73 | 2.34 | 3.66 | 3.57 | 0.11 | <0.002 | 0.60 | 99.91 |
| HMI3A* | | 58.32 | 1.40 | 16.36 | 8.86 | 0.12 | 3.70 | 6.48 | 3.02 | 1.79 | 0.29 | - | - | 100.34 |
| HMI5A* | | 64.15 | 0.66 | 15.20 | 5.60 | 0.07 | 3.60 | 2.93 | 3.40 | 2.94 | 0.13 | - | - | 98.68 |
| HMI11E* | | 65.22 | 0.47 | 15.91 | 4.12 | 0.05 | 1.55 | 5.12 | 3.60 | 2.13 | 1.18 | - | - | 99.35 |
| HMI4A* | | 66.86 | 0.51 | 15.96 | 4.56 | 0.09 | 1.95 | 4.01 | 3.10 | 2.56 | 0.13 | - | - | 99.73 |
| HMI6E* | | 67.88 | 0.62 | 15.26 | 4.80 | 0.06 | 2.43 | 4.20 | 3.47 | 1.02 | 0.28 | - | - | 100.02 |
| HMI6F* | | 72.84 | 0.21 | 14.51 | 1.72 | 0.05 | 0.69 | 2.47 | 3.11 | 3.61 | 0.04 | - | - | 99.25 |
| K2C | Mafic granulites | 55.78 | 0.53 | 16.82 | 7.52 | 0.16 | 5.49 | 6.86 | 3.34 | 2.14 | 0.07 | 0.010 | 1.00 | 99.85 |
| K6D | | 49.61 | 1.89 | 13.49 | 15.79 | 0.23 | 6.41 | 10.88 | 0.90 | 0.24 | 0.21 | 0.033 | 0.00 | 99.81 |
| K47A | | 47.42 | 0.90 | 11.83 | 14.32 | 0.29 | 14.65 | 6.84 | 0.54 | 2.05 | 0.09 | 0.155 | 0.50 | 99.71 |
| K47B | | 55.08 | 0.66 | 11.87 | 10.91 | 0.20 | 11.77 | 6.26 | 0.55 | 1.47 | 0.08 | 0.139 | 0.70 | 99.76 |
| HMI11V | | 48.63 | 1.52 | 13.74 | 15.90 | 0.24 | 5.98 | 10.51 | 2.33 | 0.50 | 0.13 | 0.013 | 0.20 | 99.82 |
| HMI11V1 | | 46.96 | 1.50 | 13.55 | 16.01 | 0.25 | 6.34 | 10.94 | 2.31 | 0.53 | 0.13 | 0.014 | 1.20 | 99.82 |
| HMI1B* | | 46.76 | 1.32 | 15.83 | 15.62 | 0.24 | 6.95 | 11.62 | 1.15 | 0.43 | 0.11 | - | - | 100.03 |
| HMI9D* | | 49.32 | 0.77 | 12.54 | 13.35 | 0.24 | 8.57 | 11.44 | 2.49 | 0.93 | 0.07 | - | - | 99.72 |
| HMI11A* | | 50.92 | 1.49 | 14.51 | 12.70 | 0.20 | 6.96 | 9.34 | 2.36 | 0.91 | 0.17 | - | - | 99.56 |
| HMI5B* | | 51.11 | 1.45 | 13.82 | 15.30 | 0.25 | 5.80 | 9.57 | 2.78 | 0.35 | 0.13 | - | - | 100.56 |
| HMI3B* | | 56.20 | 1.11 | 16.70 | 8.47 | 0.14 | 4.15 | 7.08 | 3.20 | 1.63 | 0.26 | - | - | 98.94 |
| K39 | Aluminous granulites | 49.83 | 1.32 | 16.57 | 15.57 | 0.25 | 7.42 | 5.96 | 1.99 | 0.38 | 0.11 | 0.047 | 0.20 | 99.79 |
| K46A | | 61.35 | 1.60 | 12.95 | 12.57 | 0.15 | 4.39 | 4.27 | 1.97 | 0.20 | 0.20 | 0.006 | 0.00 | 99.81 |
| K58A | | 60.26 | 0.40 | 14.75 | 14.11 | 0.22 | 5.56 | 2.09 | 1.73 | 0.62 | 0.06 | 0.049 | 0.20 | 99.79 |
| HMI9B | | 73.62 | 0.27 | 13.10 | 4.57 | 0.15 | 1.45 | 1.88 | 3.02 | 1.62 | 0.02 | 0.022 | 0.10 | 99.98 |

* Chemical analyses published by Jordt-Evangelista (1996).

Table 1- Part I I - Chemical analyses of selected samples of the Pedra Dourada Granulite.

| | | **Trace elements (ppm)** | | | | | | | | | | | |
|---|---|---|---|---|---|---|---|---|---|---|---|---|---|
| **Sample** | **Lithotype** | **Ba** | **Ce** | **Co** | **Cr** | **Cu** | **Nb** | **Ni** | **Sc** | **Sr** | **Y** | **Zn** | **Zr** |
| K5C2 | Bt-grt felsic Granulites | 164 | 51 | 117 | - | 6 | <5 | <20 | 2 | 226 | 12 | 17 | 88 |
| K52A | | 1112 | 126 | 91 | - | 17 | 5 | <20 | 3 | 409 | 9 | 38 | 233 |
| K64A | | 796 | 201 | 84 | - | 34 | 12 | <20 | 5 | 218 | 32 | 58 | 111 |
| HMI15B* | | 1431 | 154 | 23 | 20 | 7 | 5 | 14 | 3 | 421 | 6 | 40 | 274 |
| HMI7A* | | 472 | 167 | 17 | 15 | 45 | 8 | 16 | 4 | 186 | 30 | 40 | 194 |
| HMI12G* | | 755 | 40 | 13 | 9 | 0 | 0 | 8 | 4 | 124 | 33 | 0 | 37 |
| HMI12C* | | 731 | 55 | 13 | 13 | 0 | 3 | 8 | 5 | 114 | 20 | 0 | 41 |
| HMI6D* | | 752 | 172 | 1 | 12 | 0 | 3 | 23 | 2 | 167 | 30 | 12 | 269 |
| HMI11C* | | 943 | 127 | 0 | 9 | 0 | 5 | 3 | 9 | 109 | 85 | 12 | 233 |
| K1B2 | Opx felsic Granulites | 1068 | 39 | 94 | - | 9 | 9 | 21 | 8 | 407 | 12 | 66 | 182 |
| K2E | | 660 | 44 | 83 | - | 22 | 8 | <20 | 10 | 379 | 10 | 87 | 307 |
| K11A | | 1201 | 63 | 90 | - | 12 | 6 | <20 | 12 | 382 | 23 | 58 | 198 |
| K40B | | 336 | 43 | 126 | - | 18 | 9 | 20 | 6 | 253 | 11 | 51 | 78 |
| K55A | | 379 | <30 | 79 | - | 15 | <5 | <20 | 11 | 699 | 5 | 81 | 134 |
| HMI6C | | 2114 | 194 | <20 | - | 11 | 11 | <20 | 8 | 376 | 28 | 71 | 397 |
| HMI8A1 | | 1871 | 138 | 88 | - | <5 | <5 | <20 | 3 | 569 | 7 | 52 | 226 |
| HMI3A* | | 858 | 63 | 26 | 74 | 28 | 8 | 45 | 17 | 470 | 20 | 88 | 189 |
| HMI5A* | | 799 | 257 | 20 | 52 | 5 | 13 | 48 | 11 | 298 | 18 | 70 | 305 |
| HMI11E* | | 232 | 133 | 11 | 26 | 189 | 19 | 37 | 12 | 120 | 155 | 46 | 64 |
| HMI4A* | | 806 | 74 | 21 | 45 | 15 | 8 | 25 | 13 | 320 | 16 | 56 | 138 |
| HMI6E* | | 457 | 210 | 1 | 56 | 2 | 6 | 56 | 8 | 286 | 56 | 52 | 322 |
| HMI6F* | | 711 | 78 | 11 | 25 | 9 | 5 | 50 | 4 | 202 | 19 | 26 | 136 |
| K2C | Mafic Granulites | 411 | 71 | 88 | - | 53 | 8 | 77 | 20 | 381 | 34 | 104 | 94 |
| K6D | | 60 | 36 | 94 | - | 35 | 13 | 84 | 41 | 138 | 34 | 122 | 158 |
| K47A | | 175 | <30 | 94 | - | 10 | <5 | 258 | 35 | 55 | 23 | 162 | 101 |
| K47B | | 87 | <30 | 90 | - | 10 | <5 | 282 | 31 | 41 | 17 | 97 | 107 |
| HMI11V | | 62 | <30 | 78 | - | 75 | 13 | 64 | 42 | 137 | 33 | 130 | 87 |
| HMI11V1 | | 45 | <30 | 86 | - | 200 | 10 | 75 | 42 | 155 | 24 | 119 | 94 |
| HMI1B* | | 45 | 11 | 57 | 233 | 85 | 5 | 181 | 45 | 184 | 29 | 129 | 57 |
| HMI9D* | | 52 | 14 | 53 | 465 | 4 | 7 | 213 | 37 | 78 | 32 | 127 | 48 |
| HMI11A* | | 93 | 16 | 34 | 237 | 23 | 9 | 180 | 32 | 121 | 34 | 102 | 103 |
| HMI5B* | | 59 | 14 | 22 | 116 | 85 | 4 | 86 | 39 | 137 | 33 | 116 | 87 |
| HMI3B* | | 643 | 50 | 24 | 89 | 24 | 12 | 52 | 24 | 488 | 33 | 93 | 157 |
| K39 | Aluminous Granulites | 64 | <30 | 95 | - | 90 | <5 | 192 | 43 | 84 | 32 | 156 | 116 |
| K46A | | 134 | 60 | 113 | - | 11 | 20 | <20 | 30 | 58 | 52 | 154 | 276 |
| K58A | | 98 | 68 | 138 | - | 68 | <5 | 160 | 24 | 59 | 30 | 93 | 107 |
| HMI9B | | 639 | <30 | <20 | - | 26 | <5 | 62 | 14 | 174 | 45 | 45 | 240 |

* Chemical analyses published by Jordt-Evangelista (1996).

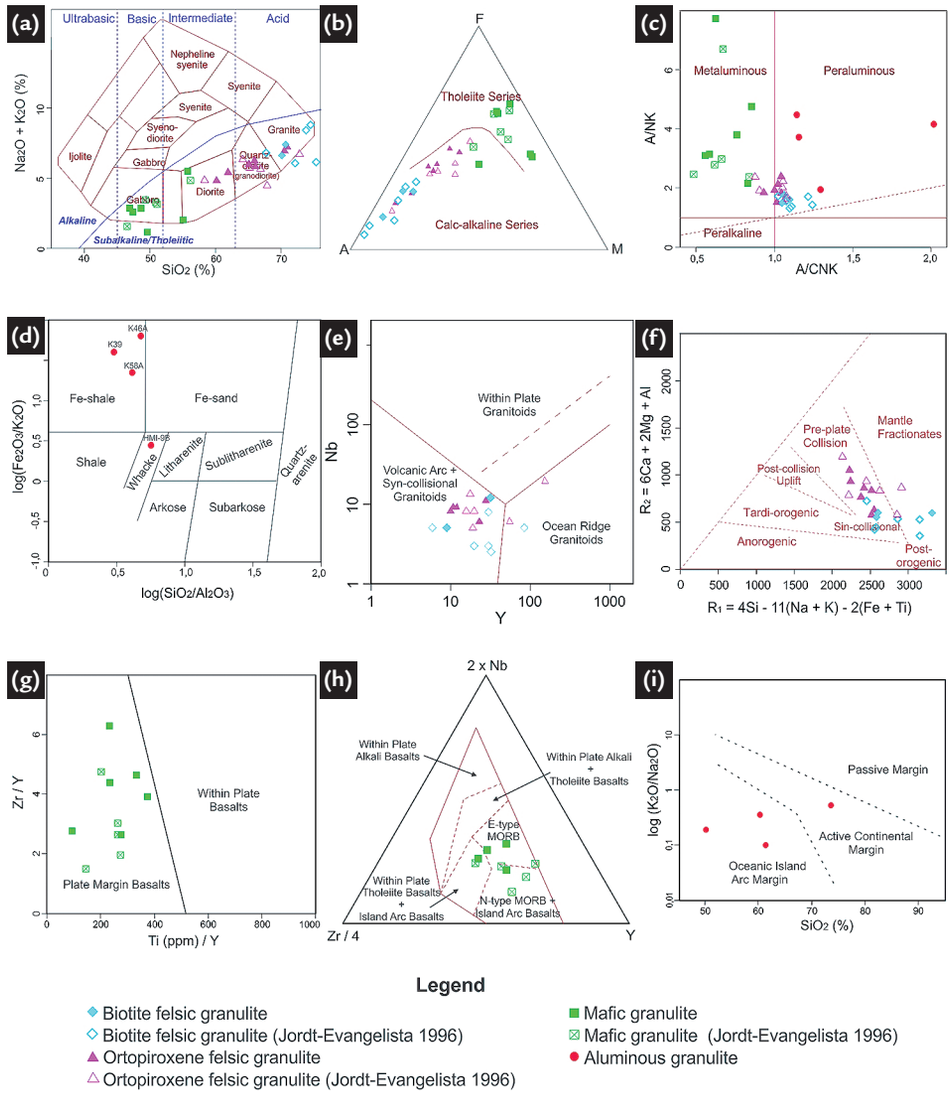


Figure 5
Chemical classification diagrams: a) TAS (Cox *et al.*, 1979); b) AFM [($Na_2O$+$K_2O$) – FeOt – MgO] (Irvine & Baragar, 1971); c) Aluminium saturation index (Shand, 1943); d) log($SiO_2$/$Al_2O_3$) versus log($Fe_2O_3$/$K_2O$) (Herron, 1988); Tectonic discrination diagrams: e) Y x Nb (Pearce *et al.*, 1984); f) R1-R2 (Batchelor & Bowden, 1985); g) Ti/Y x Zr/Y (Pearce & Gale 1977); h) Zr-Nb-Y(Meschede, 1986). i) $SiO_2$ x log($K_2O$/$Na_2O$) diagram for sandstones and argilites (Roser & Korsch, 1986).

IBC-paths are the retrograde segments of clockwise or counter-clockwise *P-T* paths (Best, 2003). The clockwise type is associated to granulite terrains generated at the base of thickened crust (doubled-crust) and require a second orogeny to uplift and expose them. The counter-clockwise *P-T* path is interpreted as a result of magmatic underplating or extension of a normal-thickness crust (single crust) (Ellis, 1987; Harley, 1989; Spear, 1992).

The chemical classification diagrams suggest that the felsic granulites protoliths are granodiorites, granites and diorites. They are predominantly peraluminous rocks belonging to calc-alkaline series. The tectonic discrimination diagrams point to convergent margin tectonic settings to the felsic granulites.

The mafic granulites protholits are gabbros and subordinate diorites. They are metaluminous rocks and have a tholeiitic character. The discriminant diagrams suggest that the mafic protholits were associated to plate boundary environments. However, these plots could not defined if they were convergent or divergent tectonic settings, as the samples show both island arcs and MORB signatures.

The aluminous granulites are peraluminous rocks with protholits that show compositional similarities with modern shales and wackes. According to the tectonic discrimination diagram, they have signatures analogous to convergent setting sediments.

## 7. Conclusions

The mineral assemblages indicate that the Pedra Dourada Granulite was metamorphosed under medium-*P* granulite-facies conditions and retrometamorphosed under greenschist- to amphibolite-facies conditions, as indicated by the secondary mineral assemblages. The chemical composition of the studied samples shows that the protoliths are acid, intermediary, and basic igneous rocks of calcalkaline or tholeiitic signature, besides the peraluminous sedimentary rocks. The tectonic discrimination diagrams suggest that these lithologies could be associated with convergent tectonic settings, wherein the mafic granulites may also be linked to extensional environments. The coronitic garnet textures present in the granulite-facies rocks suggest a near-isobaric cooling (IBC-path) after the metamorphic peak (Ellis, 1987; Harley, 1989). Based on the tectonic setting of the Pedra Dourada Granulite, this P-T path could be related to crustal thickening during the Transamazonian tectonothermal events (2,1-2,0 Ga) or the Brasiliano tectonothermal events (590-574 Ma) (Noce *et al.*, 2007). Further petrological studies and geochronological data may help to decipher the role of each event on the genesis and exhumation of the granulite terrains.

## 8. Acknowledgments

The authors are grateful to the Fundação de Desenvolvimento da Pesquisa de Minas Gerais (FAPEMIG) for financial support (research project CRA-APQ-02206-11) and to the Departamento de Geologia of the Universidade Federal de Ouro Preto for laboratory support. The first author acknowledges CAPES for the scholarship.

## 9. References

ALCÂNTARA, A.M., MACHADO, R.A. ***Cartografia geológica da quadrícula 43-03-11, escala 1:25.000 da folha Dom Silvério, MG - Subprojeto Dom Silvério.*** Ouro Preto: Universidade Federal de Ouro Preto, 2010. 58p. (Monografia).

ALKMIM, F.F., PEDROSA-SOARES, A.C., NOCE, C.M., CRUZ, S.C.P. Sobre a evolução tectônica do Orógeno Araçuaí - Congo ocidental. ***Geonomos***, v. 15, n. 1, p. 25-43, 2007.

ALMEIDA, F.F.M. O Cráton do São Francisco. ***Revista Brasileira de Geociências***, v. 7, p. 349-364, 1977.

BATCHELOR, R.A., BOWDEN, P. Petrogenetic interpretation of granitoid rock series using multicationic parameters. ***Chemical Geology***, v. 48, p. 43-55, 1985.

BEST, M.G. ***Igneous and metamorphic petrology***. (2 ed.). Massachusetts: Blackwell Science Ltd., 2003. 729p.

BRANDALISE, L. A. ***Programa Levantamentos Geológicos Básicos do Brasil. Folha Ponte Nova, SF.23-X-B-II. Escala 1:100.000.*** Brasília: DNPM/CPRM, 1991. 194 p.

COX, K.G., BELL, J.D., PANKHURST, R.J. ***The interpretation of igneous rocks***. London: George Allen & Unwin, 1979. 450p.

DE LA ROCHE, H., LETERRIER, J., GRANDCLAUDE, P., MARCHAL, M. A classification of volcanic and plutonic rocks using R1R2 diagram and major--element analyses - Its relationships with current nomenclature. ***Chemical Geology,*** v. 29, p. 183-210, 1980.

ELLIS, D.J. Origin and evolution of granulites in normal and thickened crusts. ***Geology***, v. 15, p. 167-170, 1987.

FROST, B.R., BARNES, C.G., COLLINS, W.J., ARCULUS, R.J., ELLIS, D.J., FROST, C.D. A geochemical classification for granitic rocks. ***Journal of Petrology***, v. 42, n. 11, p. 2033-2048, 2001.

HARLEY, S.L. The origins of granulites: a metamorphic perspective. ***Geological Magazine,*** v. 126, n. 3, p. 215-247, 1989.

HERRON, M.M. Geochemical classification of terrigenous sands and shales from core of log data. ***Journal of Sedimentary Petrology,*** v. 58, n. 5, p. 820-829, 1988.

IRVINE, T. N., BARAGAR, W.R.A. A guide to the chemical classification of the common volcanic rocks. ***Canadian Journal of Earth Sciences,*** v. 8, p. 523-548, 1971.

JORDT-EVANGELISTA, H. ***Petrologische untersuchungen im Gebiete zwischen Mariana und Ponte Nova, Minas Gerais, Brasilien.*** Alemanha: Universidade Técnica de Clausthal, 1984. 183p. (Ph.D. thesis).

JORDT-EVANGELISTA, H. Petrologia de fases, geotermometria e geobarometria do Complexo Granulítico de Acaiaca, Sudeste do Quadrilátero Ferrífero, MG. In: SIMPÓSIO DE GEOLOGIA DE MINAS GERAIS, 3. ***Anais...*** Belo Horizonte: SBG/Núcleo MG, 1985. p. 165-178.

JORDT-EVANGELISTA, H. O Grupo Dom Silvério, SE de Minas Gerais: petrografia, metamorfismo, geoquímica e geologia econômica. ***REM – Revista Escola de Minas,*** v. 45, n. 1-2, p.140-142, 1992.

JORDT-EVANGELISTA, H. Igneous charnockites in the southeastern transition zone between the São Francisco Craton and the Costeiro Mobile Belt, Brazil. ***Revista Brasileira de Geociências,*** v. 26, n. 2, p. 93-102, 1996.

JORDT-EVANGELISTA, H., MULLER, G. Petrology of a transition zone between the Archean Craton and the Coast Belt, SE of the Iron Quadrangle, Brazil. ***Chemie der Erde,*** v. 45, p. 129-145, 1986a.

JORDT-EVANGELISTA, H., MULLER, G. Petrologia da Zona de Transição entre o Cráton do São Francisco e o Cinturão Móvel Costeiro na Região Sudeste do Quadrilátero Ferrífero, MG. In: CONGRESSO BRASILEIRO DE GEOLOGIA, 34. ***Anais...*** Goiânia: SBG, 1986b. p. 1471-1479.

LEAKE, B.E., WOOLEY, A.R., ARPS, C.E.S., BIRCH, W.D., GILBERT, M.C., GRICE, J.D., HAWTHORNE, F.C., KATO, A., KISCH, H.J., KRIVOVICHEV, V.G., LINTHOUT, K., LAIRD, J., MANDARINO, J.A., MARESCH, W.V., NICKEL, E.H., SCHUMACHER, J., SMITH, J.C., STEPHENSON, N.C. N., UNGARETTI, L., WHITTAKER, E.J.W., YOUZHI, G. Nomenclature of Amphiboles: Report of the Subcommittee on Amphiboles of the International Mineralogical Association Commission on New Minerals and Mineral Names. ***Mineralogical Magazine,*** v. 61, p. 295-321, 1997.

MAJI, A.K., GOONA, S., BHATTACHARYA, A., MISHRA, B., MAHATO, S., HEINZ-J., BERNHARDT. Proterozoic polyphase metamorphism in the Chhotanagpur Gneissic Complex (India), and implication for trans-continental Gondwanaland correlation. ***Precambrian Research,*** v. 162, p. 385-402, 2008.

MANIAR, P. D., PICCOLI, P. M. Tectonic discrimination of granitoids. ***Geological Society of America Bulletin,*** v. 101, p. 635-643, 1989.

MESCHEDE, M. A method of discriminating between different types of mid-ocean ridge basalts and continental tholeiites with the Nb–Zr–Y diagram. ***Chemical Geology,*** v. 56, p. 207-218, 1986.

MEDEIROS JÚNIOR, E. B. ***Petrogênese do Complexo Acaiaca, MG.*** Ouro Preto: Universidade Federal de Ouro Preto, 2009. 101p. (M.Sc. thesis).

MEDEIROS JÚNIOR, E.B., JORDT EVANGELISTA, H. Petrologia e geoquímica dos granulitos do Complexo Acaiaca, região centro-sudeste de Minas Gerais. ***REM – Revista Escola de Minas,*** v. 63, n. 2, p. 219-228, 2010.

MELO, M.G., MAIA, T.T. ***Cartografia geológica da quadrícula 43-03-14, escala 1:25.000 da folha Dom Silvério, MG - Subprojeto Dom Silvério.*** Ouro Preto: Universidade Federal de Ouro Preto, 2010. 58p. (Monografia).

NOCE, C.M., PEDROSA-SOARES, A.C., SILVA, L.C., ALKMIM, F.F. O embasamento arqueano e paleoproterozóico do Orógeno Araçuaí. ***Geonomos,*** v. 15, n. 1, p. 17-23, 2007.

PASSCHIER, C.W., TROUW, R.A.J. ***Microtectonics.*** Berlim: Springer-Verlag, 2005. 366p.

PEARCE, J. A., GALE, G.H. Identification of ore-deposition environment from trace-element geochemistry of associated igneous host rocks. ***Geological Society Special Publication,*** v. 7, p. 14-24, 1977.

PEARCE, J.A., HARRIS, N.B.W., TINDLE, A.G. Trace element discrimination diagrams for the tectonic interpretation of granitic rocks. ***Journal of Petrology,*** v. 25, p. 956-983, 1984.

PEDROSA-SOARES, A.C., WIEDEMANN-LEONARDOS, C.M. Evolution of the Araçuaí Belt and its connections to the Ribeira Belt. In: CORDANI, U.G., THOMAZ FILHO, A., CAMPOS NETO, D.A. (eds.) Tectonic Evolution of South America. Rio de Janeiro: International Geological Congress, 31, 2000. p. 265-268.

PEDROSA-SOARES, A.C., NOCE, C.M., ALKMIM, F.F., SILVA, L.C., BABINSKI, M., CORDANI, U., CASTAÑEDA, C. Orógeno Araçuaí: síntese do conhecimento 30 anos após Almeida 1977. ***Geonomos,*** v. 15, n. 1, p. 1-16, 2007.

PERES, G.G. O ***Grupo Dom Silvério na região leste de Minas Gerais: arcabouço estrutural e evolução tectônica.*** Ouro Preto: Universidade Federal de Ouro Preto, 2000. 125p. (M.Sc. thesis).

PERES, G.G., ALKMIM, F.F., JORDT-EVANGELISTA, H. The southern Araçuaí belt and the Dom Silvério Group: geologic architecture and tectonic significance. ***Anais da Academia Brasileira de Ciências,*** v. 76, n. 4, p. 771-790, 2004.

ROSER, B. P., KORSCH, R. J. Determination of tectonic setting of sandstone-mudstone suites using SiO2 content and K2O/Na2O ratio. ***Journal of Geology,*** v. 94, p. 635-650, 1986.

SEN, S.K., BHATTACHARYA, A. Post-peak pressure–temperature fluid history of the granulites around Saltora, West Bengal. ***Procedures National Academy***

***Sciences India,*** v. 63, p. 282–306, 1993.

SHAND, S.J. ***Eruptive rocks. Their genesis, composition, classification and their relation to ore-deposits with a chapter on meteorite.*** New York: John Wiley & Sons, 1943. 444p.

SPEAR, F.S. Thermobarometry and P-T paths from granulite facies rocks: an introduction. Precambrian Research, v. 55, p. 201-207, 1992.

TEIXEIRA, W., JORDT EVANGELISTA, H., KAWASHITA, K., TAYLOR, P.N. 1987. Complexo granulítico de Acaiaca, MG: idade, petrogênese e implicações tectônicas. In: SIMPOSIO DE GEOLOGIA DE MINAS GERAIS, 4, ***Anais***... Belo Horizonte, SBG/Núcleo MG, 1987. v. 7, p. 58-71.

WILSON, M. ***Igneous Petrogenesis. A global tectonic aproach.*** London: Unwin Hyman, 1989. 466p.

YARDLEY, B.W.D. ***Introdução à petrologia metamórfica.*** (2ed.). Brasília: Editora Universidade de Brasília, 2004. 432p. (Tradução: FUCK, R.A.).

Received: 26 September 2014 - Accepted: 26 May 2016.